ORIGINAL PAPER

Time-resolved FRET fluorescence spectroscopy of visible fluorescent protein pairs

A. J. W. G. Visser · S. P. Laptenok · N. V. Visser ·
A. van Hoek · D. J. S. Birch · J.-C. Brochon ·
J. W. Borst

Abstract Förster resonance energy transfer (FRET) is a powerful method for obtaining information about small-scale lengths between biomacromolecules. Visible fluorescent proteins (VFPs) are widely used as spectrally different FRET pairs, where one VFP acts as a donor and another VFP as an acceptor. The VFPs are usually fused to the proteins of interest, and this fusion product is genetically encoded in cells. FRET between VFPs can be determined by analysis of either the fluorescence decay properties of the donor molecule or the rise time of acceptor fluorescence. Time-resolved fluorescence spectroscopy is the technique of choice to perform these measurements. FRET can be measured not only in solution, but also in living cells by the technique of fluorescence lifetime imaging microscopy (FLIM), where fluorescence lifetimes are determined with the spatial resolution of an optical microscope. Here we focus attention on time-resolved fluorescence spectroscopy of purified, selected VFPs (both single VFPs and FRET pairs of VFPs) in cuvette-type experiments. For quantitative interpretation of FRET–FLIM experiments in cellular systems, details of the molecular fluorescence are needed that can be obtained from experiments with isolated VFPs. For analysis of the time-resolved fluorescence experiments of VFPs, we have utilised the maximum entropy method procedure to obtain a distribution of fluorescence lifetimes. Distributed lifetime patterns turn out to have diagnostic value, for instance, in observing populations of VFP pairs that are FRET-inactive.

The more you see: spectroscopy in molecular biophysics.

To Marcus A. Hemminga on the occasion of his retirement after 40 years of research in molecular biophysics.

A. J. W. G. Visser (✉) · S. P. Laptenok ·
N. V. Visser · A. van Hoek · J. W. Borst
Microspectroscopy Centre, Wageningen University,
P.O. Box 8128, 6700 ET Wageningen, The Netherlands
e-mail: antoniejvisser@gmail.com; Ton.Visser@wur.nl

A. J. W. G. Visser · J. W. Borst
Laboratory of Biochemistry, Wageningen University,
P.O. Box 8128, 6700 ET Wageningen, The Netherlands

S. P. Laptenok · N. V. Visser · A. van Hoek
Laboratory of Biophysics, Wageningen University,
P.O. Box 8128, 6700 ET Wageningen, The Netherlands

A. J. W. G. Visser · D. J. S. Birch
Department of Physics, University of Strathclyde, Scottish
Universities Physics Alliance, Photophysics Group,
Glasgow G4 0NG, UK

J.-C. Brochon
Laboratoire de Biotechnologies et de Pharmacologie Génétique
Appliquée, Ecole Normale Supérieure de Cachan,
94235 Cachan, France

Introduction

The organisation and dynamics of biological systems rely on an intimate interplay of (biomacro-)molecules. Proteins, nucleic acids and other molecular compounds such as membrane phospholipids may interact with each other to transduce signals or to build up macromolecular structures that shape cells and intracellular organelles. Cell

functioning largely depends on protein interaction networks or, as outlined in Alberts (1998), 'the entire cell can be viewed as a factory that contains an elaborate network of interlocking assembly lines, each of which is composed of a set of large protein machines'. Unraveling protein interaction patterns is therefore of key importance to increase our understanding of cellular processes. Within the fields of genomics and proteomics, several techniques and methods have been developed including sequencing to yeast two/three hybrid methods, mass spectrometry and DNA/protein arrays to considerably increase our knowledge in the organisation of a biological system. It remains, however, necessary to develop alternative techniques and methods for visualisation and identification of interacting biomolecules in living cells. Only then will it be possible to examine the dynamics of cellular function in a spatial and temporal fashion. This will, in turn, lead to better insight into the mechanisms that systematically control the state of the cell. Combining knowledge from the fields of cell biology and biophysics may bring us an important step forward. To that end, modern microspectroscopic techniques are the methods of choice, as these techniques provide direct information on molecular interactions and dynamic events with minimum perturbation of cellular integrity and function. Microspectroscopy can be considered as a combination of microscopic and spectroscopic techniques, and it has the advantage of providing better optical contrast modes in microscopy. In this way identification and quantification of biological processes can be visualised in their natural environment. This has been established by combining two outstanding methodologies during the last decade, namely fluorescence-detected Förster resonance energy transfer (FRET) and visible fluorescent protein (VFP) technology.

FRET is a photophysical process where the excited-state energy from a donor molecule is transferred non-radiatively to an acceptor molecule at close distance via weak dipole–dipole coupling. The theory for resonance energy transfer was developed by Förster (1948). Since the transfer rate is proportional to the inverse 6th power of the distance R between donor and acceptor, the transfer rate is an extremely sensitive parameter for obtaining distances between 1 and 10 nm, far below the optical diffraction limit. The distance at which the excitation energy of the donor is transferred to the acceptor with probability 0.5 is called the Förster distance, R_0, and can be calculated using the relevant spectroscopic properties of the participating fluorophores. FRET is used extensively for monitoring interactions and conformational changes between or within biological macromolecules conjugated with suitable donor–acceptor pairs. There are several methods available for quantification of FRET, of which the one based on donor fluorescence lifetimes is the most straightforward. Fluorescence lifetimes are characterised by the average

time that a molecule remains in the excited state, which is a concentration-independent property. Donor fluorescence lifetimes in the absence and presence of acceptor molecules are often measured for the observation of FRET and a decreased fluorescence lifetime of the donor is an indication of molecular interactions. However, in cellular systems, these lifetimes may originate from interacting and non-interacting molecules, which hamper quantitative interpretation of FRET data. We have shown recently that monitoring and analyzing the time-dependent rise of acceptor fluorescence is an alternative method to circumvent this problem (Borst et al. 2008).

Time-resolved fluorescence spectroscopy already possesses a long history in the characterization of fluorescent molecules in solution. This methodology has also been applied in microscope systems where fluorescence lifetime imaging microscopy (FLIM) is now an established imaging technique. By using FLIM maps of fluorescence lifetimes of specimens can be created at 250-nm spatial resolution, i.e. close to the optical diffraction limit, and at (sub-) nanosecond temporal resolution. The FRET method and applications have been amply reviewed during the last 5 years (Jares-Erijman and Jovin 2003, 2006; Vogel et al. 2006; Elder et al. 2009). In the beginning of 2009, the proceedings of the first international Theodor Förster lecture series, held in Cambridge UK, were published offering a wealth of information on state-of-the-art quantitative optical microscopy (Kaminski 2009). Recent reviews on fluorescence lifetime imaging and on FRET–FLIM with many back references have also appeared in current literature (Festy et al. 2007; Barber et al. 2009).

To monitor cellular responses and processes using FRET, genetically encoded pairs of fluorescent proteins are of essential importance. One such genetically encoded fluorescent probe is the green fluorescent protein (GFP) from the jellyfish *Aequorea victoria*. The application of the GFP technology for imaging of intracellular proteins has been comprehensively reviewed by Tsien, the 2008 Nobel laureate (Tsien 1998). Currently a whole palette of fluorescent proteins, also from coral species, emitting from violet to red are applied extensively as genetically encoded, brightly fluorescent markers in cell biology (Zhang et al. 2002; Miyawaki et al. 2003; Shaner et al. 2004, 2005; Verkhusha and Lukyanov 2004; Giepmans et al. 2006). Thus far, the enhanced forms of cyan fluorescent protein (ECFP) and yellow fluorescent protein (EYFP) are the most commonly used FRET pair in cell biology. ECFP, however, has the disadvantage that the fluorescence decay is heterogeneous. This observation is due to the fact that ECFP can exist in two major populations where the fluorescence of the chromophore in one conformation is more quenched than the one in the other conformation (Bae et al. 2003; Borst et al. 2005). Another frequently used

combination is EGFP and the red fluorescent protein (RFP). Studies of proteins tagged with EGFP and monomeric RFP (mRFP) have already shown the potential use of this pair for FRET–FLIM applications (Peter et al. 2005; Tramier et al. 2006; Albertazzi et al. 2009).

The GFP technology has also been utilised in the development of genetically encoded FRET biosensors. The important benefit of FRET biosensors is that donor and acceptor fluorescence intensities can be measured simultaneously in two different detection channels of a fluorescence microscope enabling ratio imaging in real time. Different FRET biosensors have been developed, such as the 'cameleons' for in vivo measurements of calcium concentrations. Calcium is a very important ion second messenger in cellular signaling. Ca^{2+} signals are found in the cytosol and different organelles, but these signals are often difficult to measure by conventional fluorescent indicators. The yellow cameleon fluorescent calcium indicators are the most suitable reporters for in vivo detection of calcium because they do not require any cofactors and can be targeted to specific intracellular locations (Miyawaki et al. 1997, 1999). Several different variants of yellow cameleons have been constructed but all consist of a tandem fusion of ECFP, a calmodulin domain having four calcium binding sites, a calmodulin binding peptide M13 and EYFP (Miyawaki et al. 1997; Varadi and Rutter 2002). The level of intramolecular FRET is dependent on the extent of Ca^{2+} binding to the calmodulin. Binding of calcium ions makes calmodulin wrap around the M13 domain resulting in an increase in the FRET efficiency. The dynamic Ca^{2+} concentration range of these cameleons ranges from 10^{-8} to 10^{-2} M. Many variants of the cameleon sensors are currently available and are continuously being improved (Nagai et al. 2004). Other FRET biosensors have been developed for measuring chloride ('clomeleon') (Jose et al. 2007) and pH ('pHlameleon') (Esposito et al. 2008).

In this contribution, we focus attention on single-photon timing spectroscopy of purified VFPs in cuvette-type experiments. For quantitative interpretation of FRET in cellular systems, we need details of the molecular fluorescence that can be obtained from experiments with isolated VFPs. For analysis of time-resolved fluorescence experiments of isolated VFPs, we have utilised the maximum entropy method (MEM) (Livesey and Brochon 1987; Brochon 1994). The classical description of the fluorescence decay by a discrete set of fluorescence lifetimes has some distinct disadvantages. A well-known example, for instance, is that a fluorescence decay consisting of five exponentials with separated time constants can be fitted equally well to three exponentials with different time constants. In the case of MEM analysis, the inverse Laplace transform of the fluorescence decay is recovered by fitting the decay (and rise when appropriate) to a function composed of a large number

(up to 300) of exponentials. The advantage of MEM analysis is that we obtain a unique solution without encoding a priori information into the distribution model. Early examples of the MEM approach have been given for tryptophan fluorescence decay in a protein (Merola et al. 1989) and for flavin fluorescence decay in flavoproteins (Bastiaens et al. 1992a, b; van den Berg et al. 1998, 2001). We illustrate our approach with selected examples of VFPs and FRET pairs of VFPs.

Materials and methods

Materials

The YC3.60 was isolated and purified as previously described (Borst et al. 2008). The concentration of YC3.60 was determined with light absorption measurements at 514 nm using the YFP Venus extinction coefficient $\varepsilon = 92,200$ M^{-1} cm^{-1}. YC3.60 was diluted in 100 mM Hepes buffer at pH 7.9 containing either 50 μM EGTA alone or 50 μM EGTA and 100 μM Ca^{2+} to a final concentration of 200 nM for time-resolved fluorescence experiments. cDNA fusions of EGFP (donor) linked to mCherry (acceptor) by six amino acids (GSGSGS) [EGFP-$(L)_6$-mCherry] and ECFP (donor) coupled to EYFP (acceptor) via a 13-amino acid linker (RGGGGARDPP VAT) [ECFP-$(L)_{13}$-EYFP] and the single fluorescent proteins [ECFP, mTFP, which is monomeric teal fluorescent protein (Day et al. 2008), and EGFP] were cloned into pTYB11 vector (New England Biolabs, Impact vector system) using appropriate primers. The constructs were transformed into BL21 DE3 bacteria strain for protein expression. Expression was induced after 3 h of incubation at 37°C by adding 0.3 mM IPTG, and the cells were grown overnight at 20°C. The next day the cells were harvested and resuspended in buffer 50 mM Tris pH 8.0, 120 mM KCl, 1 mM EDTA and protease inhibitor cocktail.

Purification of VFPs

IMPACT (intein-mediated purification with an affinity chitin-binding tag) is a novel protein purification system that utilises the inducible self-cleavage activity of a protein-splicing element (called an intein) to separate the target protein from the affinity tag. In brief the following procedure was used. Bacteria expressing the fusion construct were collected by centrifugation and resuspended in 50 mM Tris pH 8.0, 120 mM KCl, 1 mM EDTA and protease inhibitor cocktail. The cells were lysed by three passages through a French pressure cell, and the homogenate was centrifuged at $20,000 \times g$ for 30 min. The soluble protein fraction was collected and applied onto an affinity matrix composed of chitin beads. The bound fusion protein

was extensively washed thereby removing other proteins and leaving the fusion-tagged protein bound to the resin. The VFPs were eluted from the tag by an on-column cleavage reaction by incubating the beads overnight in 50 mM DTT at room temperature. The purified VFP proteins were checked for purity on SDS-PAGE, and the final protein sample was transferred in the desired buffer (50 mM Tris pH 8.0, 120 mM KCl, 1 mM EDTA) via four concentration/dilution repeats using Millipore centricons. The protein concentration for time-resolved fluorescence measurements was 200 nM.

Time-resolved fluorescence experiments

Time-resolved fluorescence measurements were carried out using a mode-locked continuous wave laser for excitation and time-correlated single photon counting (TCSPC) as detection technique as extensively described previously (Borst et al. 2005, 2008). The samples were excited with plane polarised light pulses (0.2 ps FWHM) at an excitation frequency of 3.8 MHz and both parallel-polarised [$I_{//}$(t)] and perpendicular-polarised [$I_{\perp}$(t)] fluorescence intensities were detected. The fluorescence was sampled during 10 cycles of 10 s (real time) in each polarisation direction, where the detection frequency in the polarisation channel of highest intensity was set to 30 kHz to prevent pulse pileup. The time-resolved fluorescence experiments on the yellow cameleon variant YC3.60 were performed by using 400-nm excitation of ECFP and fluorescence detection of ECFP with a 480.5-nm interference filter (Schott, Mainz, Germany; half-bandwidth of 5.4 nm). The sensitised emission of YFP Venus fluorescence in YC3.60 was detected with an OG 530 cut-off filter (Schott) and 557.6-nm interference filter (Schott; half-bandwidth 5.9 nm). Experiments with the ECFP-(L)$_{13}$-EYFP construct, ECFP and mTFP were conducted at 430-nm excitation of ECFP with 480.5-nm detection of ECFP or mTFP fluorescence. We also measured the time-dependent rise of EYFP fluorescence in the ECFP-(L)$_{13}$-EYFP construct at 557.6 nm.

In all these experiments the dynamic instrumental response function of the setup was obtained at the ECFP or Venus emission wavelengths by using a solution of xanthione in ethanol as reference compound having an ultrashort fluorescence lifetime of 14 ps. EGFP and the EGFP-(L)$_6$-mCherry construct were excited at 487 nm, and the EGFP donor fluorescence was detected through the OG530 filter and a 539-nm interference filter (Schott). The sensitised mCherry fluorescence was measured through the OG530 filter and a 647-nm interference filter (Schott). The reference compound for EGFP fluorescence decay and mCherry fluorescence rise and decay was erythrosine B in aqueous solution having a fluorescence lifetime of 85 ps. One complete measurement consisted of sampling polarised fluorescence decays of the reference compound (3 cycles of 10 s in each polarisation direction), the sample (10 cycles), the background (usually 2 cycles, as it is only less than 1% of the intensity of the sample) and again the reference compound.

Data analysis in terms of discrete exponentials and distance distribution

The total experimental fluorescence $I(t)$ can be written as the convolution product of the instrumental response function IRF(t) with the model function $i(t)$:

$$I(t) = \text{IRF}(t) \otimes i(t), \tag{1}$$

in which $i(t)$ can be written as

$$i(t) = i_{//}(t) + 2gi_{\perp}(t) = \sum_{i}^{n} a_i \exp(-t/\tau_i), \tag{2}$$

with n denoting the number of exponential components with amplitudes a_i and fluorescence lifetimes τ_i. The g-factor was found to be equal to 1 in our single-photon timing apparatus (van Hoek et al. 1987) eliminating polarisation artifacts in the total fluorescence decay analysis. Fitting the fluorescence decay to a two- or three-component multi-exponential function was accomplished as described earlier (Borst et al. 2005).

The fluorescence decay of the EGFP-L$_6$-mCherry construct following excitation at 487 nm and emission at 537 nm of donor EGFP was analysed using a model for distribution of distances between the transition moments of the chromophores in EGFP and mCherry (Grinvald et al. 1972; Haas et al. 1975). The fluorescence intensity decay of the donor alone is presented by an exponential function:

$$i_D(t) = i_D(0) \exp(-t/\tau_D), \tag{3}$$

where τ_D is the fluorescence lifetime of the donor alone. The fluorescence intensity decay of the donor in the presence of acceptor can be modelled as a multi-exponential function:

$$i_{DA}(t) = i_{DA}(0) \int_{0}^{\infty} f(R) \exp\left[-\frac{t}{\tau_D} - \frac{t}{\tau_D}\left(\frac{R_0}{R}\right)^6\right] dR, \tag{4}$$

where $f(R)$ is the distribution function of donor–acceptor distances, R the actual distance and R_0 the critical (or Förster) distance between donor and acceptor. It is assumed that $f(R)$ is a Gaussian function:

$$f(R) = \frac{1}{\sigma\sqrt{2\pi}} \exp\left[-\frac{(R - <R>)^2}{2\sigma^2}\right], \tag{5}$$

where $<R>$ is the mean distance and σ the width of the distribution. R_0 has been determined as 5.2 nm. The experimental time-resolved data can be fitted to the following donor decay function:

$$i_D(t) = b_1 i_D(t) + b_2 i_{DA}(t), \qquad (6)$$

in which b_1 and b_2 are the amplitudes representing the fractions of donor molecules that are FRET-inactive and FRET-active respectively. The recovered parameters are τ_D, $<R>$, σ, b_1 and b_2.

MEM data analysis

The MEM type of analysis of time-resolved fluorescence decay data has been detailed previously (Livesey and Brochon 1987; Brochon 1994). Analysis of total fluorescence decay $I(t)$ was performed using the commercially available MEM (Maximum Entropy Solutions, Ely, UK). In all experiments, the parallel and perpendicular fluorescence intensity components were acquired after excitation with vertically polarised light. The amplitude image $\alpha(t)$ of the total fluorescence intensity $i(t)$, after δ-pulse excitation, is given by the inverse Laplace transform:

$$i(t) = i_{//}(t) + 2i_{\perp}(t) = \int_0^\infty \alpha(\tau) \exp(-t/\tau) d\tau. \qquad (7)$$

The image $\alpha(t)$ is recovered by maximising the Skilling–Jaynes entropy function S_{SJ} (Livesey and Brochon 1987):

$$S_{SJ} = \int_0^\infty \{\alpha(\tau) - m(\tau) - \alpha(\tau)\log(\alpha(\tau)/m(\tau))\}d\tau, \qquad (8)$$

and minimising the χ^2 data fit criterion

$$\chi^2 = \frac{1}{M} \sum_{k=1}^{M} \left((I_k^{calc} - I_k^{obs})/\sigma_k\right)^2, \qquad (9)$$

where $m(t)$ is the starting model of the distribution chosen to be flat in log τ space, when there is no a priori information about the system, as this would introduce the least correlation between the parameters of the image $\alpha(\tau)$. The superscripts calc and obs on I denote the observed and calculated intensities in channel k of the multichannel analyzer. M is the total number of channels used in the analysis of the fluorescence decay (typically 4,000 channels), and σ_k^2 is the variance in channel k. For an optimal fit of the data, χ^2 should approach unity. In practice, 150 (or 300) data points equally spaced on a log τ scale (between 1 ps and 10 ns) were used in the analysis of $i(t)$.

The average fluorescence lifetime is calculated from the obtained spectrum (or image) $\alpha(\tau)$ as follows:

$$<\tau> = \sum_{i}^{N} \alpha_i \tau_i / \sum_{i}^{N} \alpha_i, \qquad (10)$$

where the summation is carried out over the whole range (N) of τ_i values of an $\alpha(\tau)$ spectrum. The barycenter of a peak in the spectrum is determined in a similar fashion

except that the summation is performed over a limited range of τ_i values encompassing a local peak (Merola et al. 1989). The fractional area of a peak is the ratio between the integrated peak intensity and the total intensity of the spectrum.

In all graphs presented, the amplitude of the barycenter is given as the percentage of normalised pre-exponential factors. The time scale is logarithmic.

The experimental and fitted time-resolved fluorescence traces, which are not shown in this paper, are presented in the electronic supplementary material (ESM).

Results and discussion

Time-resolved fluorescence spectroscopy of EGFP

The MEM analysis will provide information about distributions of lifetimes in contrast to previous and more common analysis procedures using multi-exponential decay models of discrete lifetimes. The time-resolved fluorescence of the enhanced green fluorescent protein (EGFP) at pH 8.0 serves as an illustrative example. The experimental and MEM-fitted fluorescence decays of EGFP are shown in Fig. 1a, and the lifetime distribution pattern is presented in Fig. 1b. It is clear that the fluorescence decay is not completely a single exponential, since two peaks appear with barycenters at 2.63 ns (normalised amplitude 86%) and 1.36 ns (normalised amplitude 14%). This heterogeneity of time-resolved fluorescence of EGFP has been independently demonstrated before by analysis with a multi-exponential decay model with discrete lifetimes (Uskova et al. 2000; Heikal et al. 2001; Suhling et al. 2002; Hess et al. 2003). We have analysed the same experimental data with a bi-exponential decay model and incorporated the fit results as sticks of height proportional to the amplitude values in Fig. 1b showing that the agreement between both analysis methods is excellent.

Time-resolved fluorescence spectroscopy of the yellow cameleon variant: YC3.60

Donor fluorescence lifetimes in absence and presence of acceptor molecules are often measured for the observation of FRET. The FRET-based calcium sensor yellow cameleon 3.60 (YC3.60) has been investigated as a test system because it changes its conformation on calcium binding, thereby increasing the FRET efficiency. In this study, we have analysed the same experimental time-resolved fluorescence intensity data as published in Borst et al. (2008) with the MEM approach. First we analysed the fluorescence decays of ECFP (donor alone) and YC3.60 in the
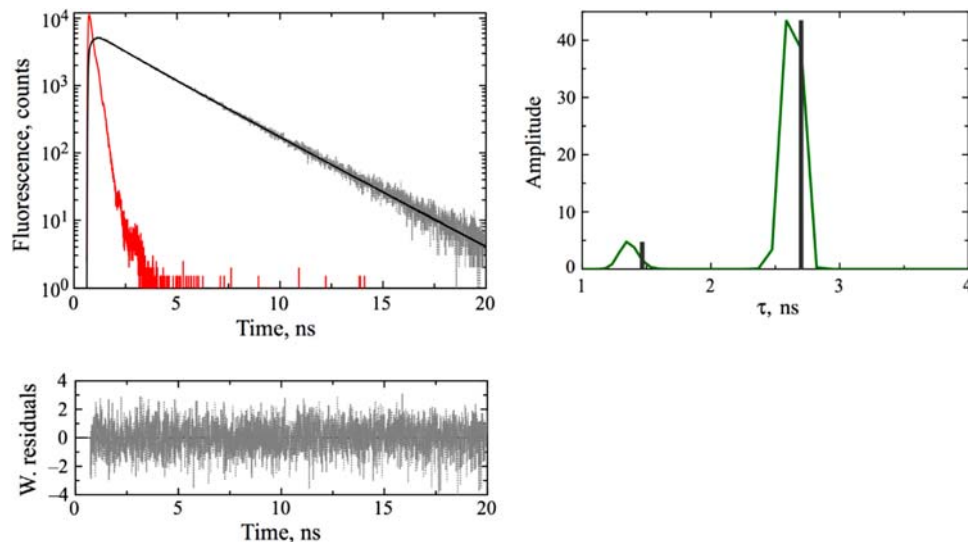
Fig. 1 Total fluorescence decay analysis of EGFP obtained with the MEM approach. Excitation and emission wavelengths were 487 and 539 nm. *Left panel* presents experimental (*grey* points) and fitted (*black solid line*) time-resolved fluorescence curves, together with the reference compound erythrosine B (*red*). To show the optimised fit, the weighted residuals between the experimental and calculated curves are shown. The fit criterion $\chi^2 = 1.05$. *Right panel* illustrates recovered lifetime distribution with barycenters at 1.36 ns (normalised amplitude 14%) and at 2.63 ns (normalised amplitude 86%) (see Table 3). Also shown in the distribution are vertical sticks (*black*) corresponding to discrete lifetime analysis of the same data located at 1.47 ns (normalised amplitude 10%) and 2.70 ns (normalised amplitude 90% and scaled to the maximum value of the barycenter). The time-scale extends between 1 ps and 10 ns. A total of 150 lifetimes were used in the distribution between 1 ps and 10 ns, of which the ones between 1 and 4 ns are shown

absence and presence of calcium ions at 400-nm excitation wavelength and 480-nm detection wavelength and using 4,000 data points in time channels incremented with 5 ps per channel. MEM analysis shows two lifetime distributions for ECFP and four separate lifetime distributions for YC3.60 as depicted together in Fig. 2a. All numerical results are collected in Table 1. The lifetime distribution of ECFP clearly consists of two major contributions, one relatively broad distribution centred at 3.2 ns covering 72% of amplitude area and one relatively sharp distribution centred at 0.95 ns with 28% of amplitude area. These results are in very good agreement with the ones obtained with analysis with discrete lifetime components, 3.57 ns (67%) and 0.97 ns (33%) respectively (Borst et al. 2008). These data are presented as sticks of relative heights together with the lifetime distribution of ECFP in Fig. 2b.

The lifetime distribution of YC3.60 in the absence of calcium is more complex and consists of three peaks located at 3.2 ns (24%), 1.9 ns (24%) and 0.73 ns (36%) and one relatively small distribution located at 90 ps (14%). The 3.2-ns peak is the same as found for ECFP and must be ascribed to a population of YC3.60 molecules not participating in FRET. The previously obtained three discrete lifetimes have been incorporated as sticks of appropriate lengths in the lifetime distribution of YC3.60 in the absence of calcium in Fig. 2c.

The agreement between both analysis results is fair, but not optimal. When we compare the MEM results of this single experiment with the ones obtained from global

analysis of many experiments in discrete lifetimes embedding the existence of two fractional populations (Borst et al. 2008), then we can tentatively assign the 1.9-ns peak to the one found previously at 2.1 ns and the 0.73-ns peak to the one found previously at 0.5 ns. The advantage of the MEM analysis is that we directly observe the lifetime components in a distribution, whereas recovery of discrete lifetimes required global analysis of many time-resolved fluorescence experiments, in which prior information on the amount of different populations (FRET-active and FRET-inactive) in the ensemble has been encoded.

The complexity of the lifetime distribution is even larger in the case of YC3.60 in the presence of calcium ions, for which five discrete lifetimes in the time domain between 1 ps and 10 ns are observed. Very pronounced, however, is the predominant (74%) lifetime distribution around 6 ps, which must be ascribed to an YC3.60 conformation having very efficient FRET. This 6-ps component is clearly absent in the discrete lifetime component analysis (see the poor agreement between both analysis methods in Fig. 2d). The advantage of the MEM analysis is that this predominant contribution is directly visible, whereas this short lifetime component remains hidden in analysis with discrete lifetimes. According to the cartoon models of YC3.60 with and without calcium as published previously, this would only be possible when the two fluorescent proteins are located next to each other (Borst et al. 2008). The non-resolved distribution in the short time domain must correspond to the predominant 24-ps lifetime component as was found
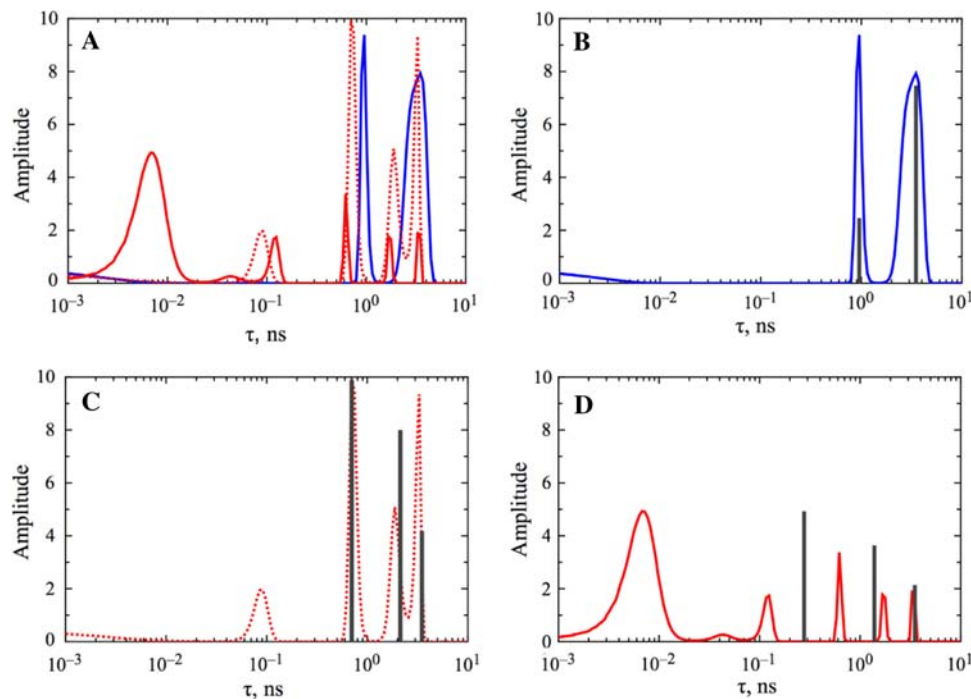
Fig. 2 a Fluorescence lifetime distribution obtained after MEM analysis of time-resolved donor fluorescence of ECFP (*blue*), Ca^{2+}-free YC3.60 (*dotted red curve*) and Ca^{2+}-bound YC3.60 (*solid red curve*). Excitation and emission wavelengths were 400 and 480 nm. The time-scale is logarithmic and extends between 1 ps and 10 ns covered by 150 lifetimes. The lifetimes and corresponding integrated amplitudes are listed in Table 1. In **b–d** the stick spectra of discrete lifetimes (in *black*) are also shown for comparison, published in Borst et al. (2008). These discrete lifetime values with amplitudes in parentheses are as follows: for ECFP 0.97 ns (33%) and 3.57 ns (67%); for Ca^{2+}-free YC3.60 0.67 ns (45%), 2.20 ns (36%) and 3.57 ns (fixed, 19%); for Ca^{2+}-bound YC3.60 0.28 ns (46%), 1.39 ns (34%) and 3.57 ns (fixed, 20%)

Table 1 Fluorescence lifetimes recovered from MEM analysis of time-resolved fluorescence of ECFP and YC3.60 in absence and presence of calcium ions

Sample	α_5	τ_5 (ns)	α_4	τ_4 (ns)	α_3	τ_3 (ns)
ECFP						
YC3.60 − Ca^{2+}			0.13 ± 0.03	0.09 ± 0.01	0.34 ± 0.05	0.73 ± 0.03
YC3.60 + Ca^{2+}	0.76 ± 0.17	0.006 ± 0.001	0.08 ± 0.03	0.12 ± 0.02	0.06 ± 0.01	0.63 ± 0.03

Sample	α_2	τ_2 (ns)	α_1	τ_1 (ns)	$<\tau>$ (ns)
ECFP	0.28 ± 0.03	0.95 ± 0.05	0.72 ± 0.04	3.2 ± 0.06	2.54 ± 0.13
YC3.60 − Ca^{2+}	0.24 ± 0.05	1.94 ± 0.19	0.23 ± 0.06	3.17 ± 0.12	1.45 ± 0.19
YC3.60 + Ca^{2+}	0.04 ± 0.00	1.72 ± 0.10	0.04 ± 0.00	3.39 ± 0.04	0.24 ± 0.03

previously in the global analysis, in which two fractional populations of FRET-active and FRET-inactive donor molecules were present. The other distributed lifetimes are difficult to assign, which was also the case for the previous analysis with discrete lifetime components, for which in three different analyses lifetimes of 1.46, 0.28 and 0.14 ns were recovered. The 3.4-ns lifetime component present in the Ca^{2+}-bound YC3.60 sample again indicates a population of YC3.60 molecules, which do not exhibit FRET. Both the heterogeneity of the fluorescence decay of ECFP and the presence of a population of non-interacting donor molecules in the construct severely complicate quantitative analysis of FRET in terms of discrete lifetimes (Millington et al. 2007; Borst et al. 2008; Wlodarczyk et al. 2008).

We previously described a methodology for the detection of FRET that monitors the rise time of acceptor fluorescence upon donor excitation, thereby detecting only those molecules undergoing FRET (Borst et al. 2008). This rise time is completely equivalent to the fluorescence lifetime of the donor in the vicinity of an acceptor molecule. The main advantage of this method, as compared to the more commonly used donor fluorescence quenching
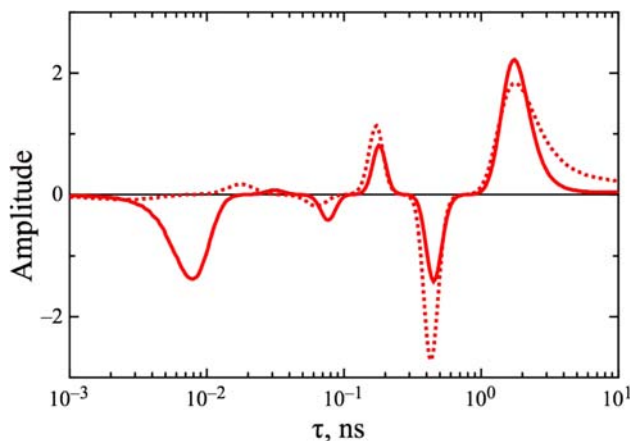
Fig. 3 Fluorescence lifetime distribution obtained after MEM analysis of time-resolved acceptor fluorescence of Ca^{2+}-free YC3.60 (*dotted red curve*) and Ca^{2+}-bound YC3.60 (*solid red curve*). Excitation and emission wavelengths were 400 and 558 nm. The time-scale extends between 1 ps and 10 ns. A total of 300 lifetimes were used in the distribution between 1 ps and 60 ns. For Ca^{2+}-free YC3.60, there are two main lifetimes at 1.82 ns (*positive* amplitude) and at 0.44 ns (*negative* amplitude). The absolute ratio of areas amounts to 1 (1.82 ns):0.45 (0.44 ns). For Ca^{2+}-bound YC3.60, three peaks can be distinguished at 2.0 ns (*positive* amplitude), 0.46 ns (*negative* amplitude) and 7 ps (*negative* amplitude), with relative areas of 1:0.34:0.83 respectively

method, is that the transfer rate of FRET can be determined accurately even in cases where the FRET efficiencies approach 100%. We have subjected selected experimental data (4,000 data points in time channels incremented with 1 ps per channel), which were previously analysed with an exponential model with rise and decay components, to the MEM analysis procedure. It was immediately apparent that the recovered lifetime distributions indeed exhibit negative amplitudes as expected with a time-dependent increase (rise) in fluorescence intensity, and positive amplitudes associated with fluorescence decay components. The results are shown in Fig. 3 for YC3.60 in the presence and absence of calcium ions.

For Ca^{2+}-free YC3.60, there are two main distributions peaked at 1.82 ns with positive amplitude and at 0.44 ns with negative amplitude. The absolute ratio of areas amounts to 2.2 in favour of the longer lifetime distribution. The lifetime with negative amplitude is a signature for the rise time. The 0.44-ns component may well correspond to the 0.73-ns component from the donor fluorescence decay. The other distributed lifetimes have much smaller contributions and are not further discussed. For Ca^{2+}-bound YC3.60, three peaks can be distinguished at 2.0 ns (positive amplitude), 0.46 ns (negative amplitude) and 7 ps (negative amplitude), with relative areas of 1, 0.34 and 0.83, respectively. This distributed 7-ps rise time found in Ca^{2+}-bound YC3.60 is in complete agreement with the presence of the very short distributed lifetime of the donor

fluorescence decay, which is characteristic for very efficient FRET (Fig. 2d). The distribution with positive amplitude arises from the decay of the acceptor (Venus) fluorescence. This fluorescence lifetime amounts to 3.1 ns as determined from experiments at longer time scales (Borst et al. 2008). A 3.1-ns lifetime would not be recovered after MEM analysis of experimental time-resolved fluorescence data in the 4-ns time range.

Time-resolved fluorescence spectroscopy of the construct ECFP-(L)$_{13}$-EYFP

We are interested to observe whether the presence of a population of FRET-inactive molecules is a general property of ECFP-EYFP couples. For that reason we have also included a control FRET construct composed of a flexible linker of 13 amino acids with ECFP and EYFP at both ends. The MEM analysis yields lifetime distribution patterns of ECFP and ECFP-(L)$_{13}$-EYFP, which are presented in Fig. 4. The numerical results have been collected in Table 2. The short fluorescence lifetime distribution of ECFP (0.95 ns, see Fig. 2b, Table 1) has been further resolved in lifetimes of 0.87 ns and 1.64 ns of about equal amplitudes. It is to be noted, however, that the excitation wavelength was at 430 nm instead at 400 nm and that the buffer composition was also different as compared to the previous experiment with ECFP. This resolution in three lifetime components instead of two using the MEM approach has been observed before and illustrates again that the ECFP fluorescence decay is heterogeneous and the distributed lifetimes are sensitive to external factors (Villoing et al. 2008). MEM analysis of the donor fluorescence decay in the FRET
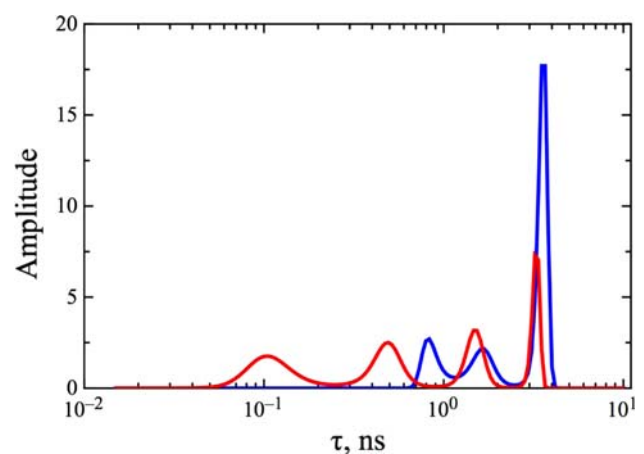

Fig. 4 Fluorescence lifetime distribution obtained after MEM analysis of time-resolved donor fluorescence of ECFP (*blue*) and ECFP-L$_{13}$-EYFP (*red*). Excitation and emission wavelengths were 430 and 480 nm. The time-scale extends between 10 ps and 10 ns covering 150 lifetimes. The lifetimes and corresponding integrated amplitudes are listed in Table 2

Table 2 Fluorescence lifetimes recovered from MEM analysis of time-resolved fluorescence of ECFP and ECFP-L$_{13}$-EYFP

Sample	α_4	τ_4 (ns)	α_3	τ_3 (ns)	α_2	τ_2 (ns)	α_1	τ_1 (ns)	$<\tau>$ (ns)
ECFP			0.17 ± 0.07	0.87 ± 0.13	0.19 ± 0.08	1.64 ± 0.32	0.64 ± 0.04	3.52 ± 0.08	2.71 ± 0.01
ECFP-L$_{13}$-EYFP	0.29 ± 0.04	0.12 ± 0.01	0.27 ± 0.04	0.49 ± 0.06	0.22 ± 0.03	1.49 ± 0.10	0.22 ± 0.01	3.24 ± 0.06	1.19 ± 0.01

construct recovered four distributed lifetimes, where the short lifetimes (0.12 and 0.49 ns) must be ascribed to FRET, since they do not show up in the lifetime distribution of ECFP alone. The nature of the fluorescence lifetime of 1.49 ns is unknown, but it might originate from two molecular populations that are FRET-active and FRET-inactive. The fluorescence lifetime of 3.24 ns (22%) must be ascribed to a FRET-inactive population. This amount is of similar magnitude as found for the yellow cameleon in the presence and absence of calcium. From these experiments, one can conclude that FRET sensors composed of ECFP and EYFP always display a population of donor molecules, which are not involved in the FRET process.

An ECFP analogue with a single fluorescence lifetime

From the previous results, ECFP clearly showed at least two lifetime distributions indicating the existence of at least two conformations of ECFP, which has also been demonstrated in crystallography of ECFP (Bae et al. 2003). These specific ECFP conformations most likely possess different FRET efficiencies. Therefore it is highly desirable to have a FRET donor molecule with mono-exponential fluorescence decay properties for easier interpretation of the FRET data. We think that mTFP is such a candidate, since in the fluorescence lifetime distribution, a well-defined peak at 2.9 ns (91%) is apparent and only a small amount (9%) of a species with a shorter lifetime (0.91 ns) is present (Fig. 5). The more homogeneous fluorescence has also been reported previously (Day et al. 2008). For confocal imaging this fluorescent protein is also more suitable, since its excitation maximum is at 460 nm, which overlaps perfectly with the 458-nm line of an argon ion laser.

Time-resolved fluorescence spectroscopy of the construct EGFP-(L)$_6$-mCherry

Nowadays cell biologists are shifting towards applications with acceptor molecules having more red-shifted fluorescence for the observation of FRET in combination with EGFP as donor moiety because of its more mono-exponential fluorescence decay. Therefore, we have analysed the lifetime properties of a fusion construct composed of EGFP and mCherry connected by six amino acids (see "Materials" section). Also for this construct and EGFP
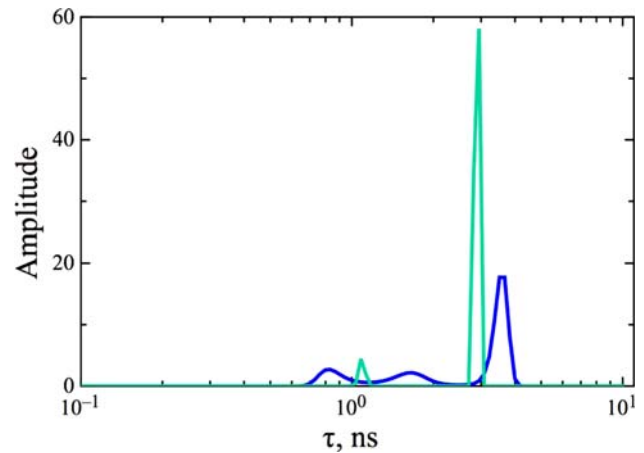

Fig. 5 Fluorescence lifetime distribution obtained after MEM analysis of time-resolved fluorescence of ECFP (*blue*) and mTFP (*green*). Excitation and emission wavelengths were 430 and 480 nm. A total of 150 lifetimes were used in the distribution in the time domain between 15 ps and 10 ns, of which the distribution between 0.1 and 10 ns is shown. The lifetimes and corresponding integrated amplitudes of ECFP are listed in Table 2. The lifetimes of mTFP are 2.89 ns (91%) and 0.91 ns (9%)
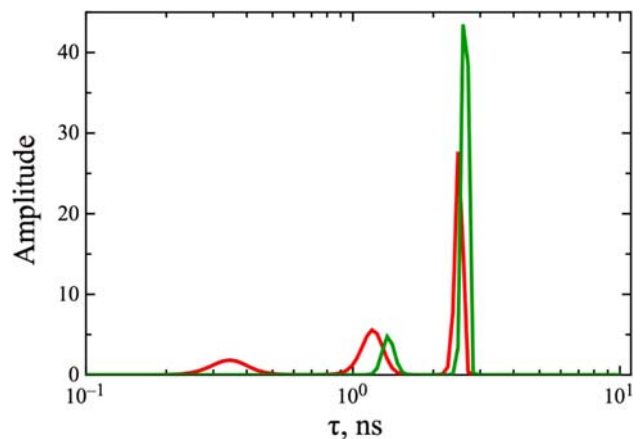

Fig. 6 Fluorescence lifetime distribution obtained after MEM analysis of time-resolved fluorescence of EGFP (*green*, see also Fig. 1) and EGFP-L$_{13}$-mCherry (*red*). Excitation and emission wavelengths were 487 and 539 nm. A total of 150 lifetimes were used in the distribution in the time domain between 15 ps and 10 ns, of which the ones between 0.1 ns and 10 ns are shown. The lifetimes and corresponding integrated amplitudes are listed in Table 3

only (see also Fig. 1a), the lifetime distributions have been obtained by MEM analysis (Fig. 6). Numerical results of analysis have been collected in Table 3. The lifetime

Table 3 Fluorescence lifetimes recovered from MEM analysis of time-resolved fluorescence of EGFP and EGFP-L$_6$-mCherry

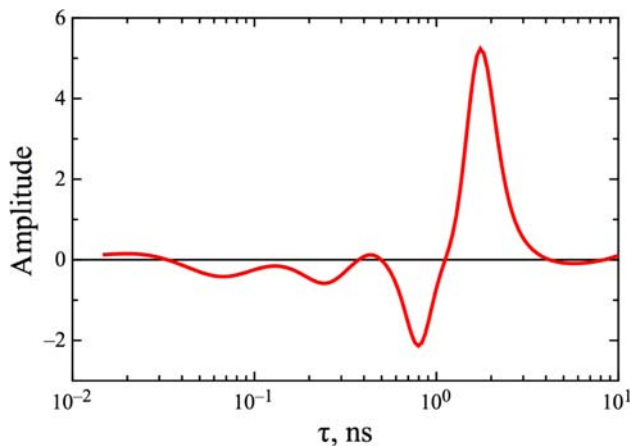| Sample	α_3	τ_3 (ns)	α_2	τ_2 (ns)	α_1	τ_1 (ns)	$<\tau>$ (ns)
EGFP			0.14 ± 0.01	1.36 ± 0.07	0.86 ± 0.02	2.63 ± 0.01	2.45 ± 0.00
EGFP-L$_6$-mCherry	0.17 ± 0.02	0.35 ± 0.05	0.30 ± 0.03	1.18 ± 0.06	0.53 ± 0.02	2.49 ± 0.02	1.73 ± 0.01

Fig. 7 Fluorescence lifetime distribution obtained after MEM analysis of time-resolved acceptor fluorescence of EGFP-L$_{13}$-mCherry. Excitation and emission wavelengths were 487 and 647 nm. The time-scale extends between 10 ps and 10 ns. A total of 150 lifetimes were used in the distribution between 15 ps and 10 ns. Lifetimes with negative amplitudes are found at 0.78 ns, 0.23 ns and 72 ps with relative areas 1:0.43:0.42 respectively. The lifetime with positive amplitude is at 1.89 ns with an absolute ratio of areas of 1 (1.89 ns):0.33 (0.78 ns)

distribution of the EGFP-(L)$_6$-mCherry construct has a pattern of three lifetimes at 2.49, 1.18 and 0.35 ns with amplitudes listed in Table 3. The short linker of six amino acids (GSGSGS) puts a constraint of relatively small distances between both fluorescent proteins (Evers et al. 2006). Because the linker peptide has a very flexible structure, it is very possible that we are facing a distribution of relative distances and orientations between both transition moments. This implies that there are at least two conformations of the construct with different transfer efficiencies. Additional support for this observation comes from the MEM analysis of the rise and decay of the acceptor fluorescence, the distribution of which is depicted in Fig. 7. It is clear from Fig. 7 that there are at least three distinct distributed rise times present at 0.78, 0.23 and 72 ps. The distributed lifetime with positive amplitude has a peak value at 1.89 ns and must be attributed to the fluorescence lifetime of the acceptor mCherry. Since it has been previously shown that the FRET process follows a static regime (i.e. the rate of conformational changes is smaller than the FRET rate) (Borst et al. 2008), the conformations are in slow equilibrium and can well be represented by a distribution of distances.

The recovery of a distance distribution from time-resolved fluorescence experiments monitoring the donor fluorescence was already addressed a few decades ago (Grinvald et al. 1972; Haas et al. 1975; Wu et al. 1991). We have analysed the time-resolved donor fluorescence in terms of a distance distribution taking into account a FRET-inactive fraction of donor molecules (see "Methods" section). Because of the flexible chain, it is assumed that the distribution function has a Gaussian form. The Förster radius for the EGFP-mCherry pair is determined as 5.2 nm and is used as an input value for the analysis. The output parameters are the Gaussian distribution, the fluorescence lifetime of donor EGFP and the fraction of FRET-inactive EGFP molecules. The analysis resulted in a distribution of distances with mean distance $<R>$ of 4.6 (±0.2) nm and width σ of 1.2 (±0.1) nm. It must be emphasised that this analysis provides an 'apparent' distribution and distance with contributions from both distance and orientation (Wu and Brand 1992). The recovered
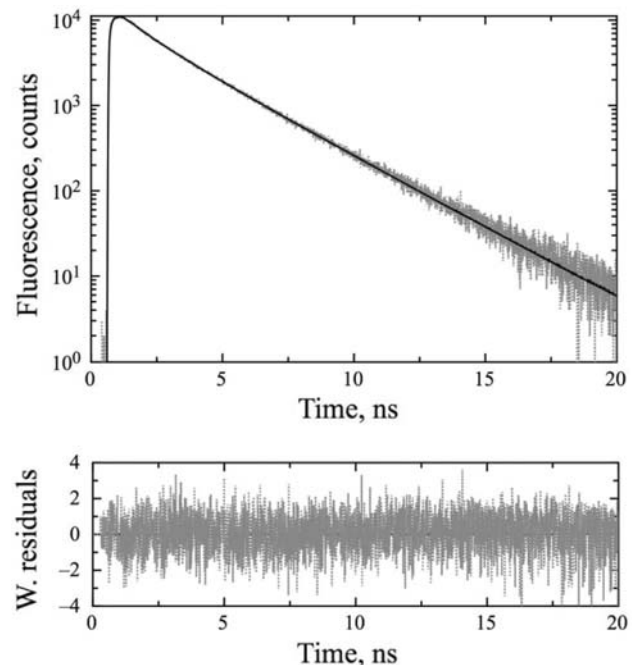

Fig. 8 Analysis of the time-resolved fluorescence of the donor (EGFP) in the construct EGFP-L$_{13}$-mCherry with a model of Gaussian distribution of distances (Eqs. 4–5) and a certain percentage of FRET-inactive EGFP (Eq. 6). The recovered parameters are $\tau_D = 2.63$ ns, $<R> = 4.6 \pm 0.2$ nm, $\sigma = 1.2 \pm 0.1$ nm, $b_1 = 48.5\%$ and $b_2 = 51.5\%$. $\chi^2 = 1.13$

fluorescence lifetime of EGFP is 2.63 ns, and the estimated fraction of non-interacting EGFP is 48%. This is close to the value found by the MEM analysis (see Table 3). Experimental results and fits are given in Fig. 8. Given the fact that the mean distance is smaller than the Förster distance, the resulting measured donor fluorescence lifetimes must be shorter than 1.3 ns as actually observed.

The high fraction of non-interacting EGFP is puzzling. The high contribution (48%) can be explained taking the presence of non-matured mCherry into account. Maeder and co-workers used a similar construct with a different linker in yeast and found that 50% of mCherry is not matured (Maeder et al. 2007). Non-matured mCherry contains green chromophores, which are different from EGFP and with shorter fluorescence lifetimes (Cotlet et al. 2001). It means that in the population of EGFP-L_6-mCherry molecules there is a mixture of directly excited non-matured mCherry and excited non-matured mCherry via resonance energy transfer from EGFP. Both components in the mixture emit fluorescence with a slightly shorter lifetime than EGFP alone. Note in this respect that the MEM analysis did not recover the 2.63-ns lifetime of free EGFP, but a distinctly shorter lifetime of 2.49 ns.

Concluding remarks

In this paper, we have shown the application and usefulness of MEM analysis of time-resolved fluorescence of VFPs. The lifetime distribution pattern obtained after MEM analysis has a clear diagnostic value. For instance, it can be immediately observed when a population of donor VFP is not participating in FRET. MEM analysis of fluorescence decay of the calcium sensor YC3.60 is in good agreement with single-component global analysis of time-resolved fluorescence with the encoding of prior information. We emphasise the large advantage of employing MEM analysis: it is not necessary to look for the number of exponential components, notably in the case of very complex fluorescence decays. Complexity arises when the donor decay is not mono-exponential, when there is a mixture of populations exhibiting FRET and no FRET or when the FRET construct has a flexible linker causing a distribution of distances in FRET pairs. Even rise components can be investigated with MEM analysis with the additional advantage that only FRET active pairs are pre-selected.

In all these VFP pairs, there is a certain percentage in the ensemble that does not give FRET. What is the reason? It should be realised that some of these fluorescent proteins are natural 'bioluminescence' resonance energy transfer (BRET) sensors. In other words they function as antenna proteins for accepting the energy that is liberated in a biochemical oxidation reaction. When these fluorescent proteins are illuminated, i.e. with many more photons than are generated in the bioluminescent reaction, they turn out to be photolabile and undergo photoconversion, which has been documented for GFP (Patterson and Lippincott-Schwartz 2002), YFP (Valentin et al. 2005; Kirber et al. 2007) and recently also for orange and red fluorescent proteins (Kremers et al. 2009). Photoconversion can also take place during the FRET process. During FRET measurements a certain percentage of photoconverted acceptor molecules can be generated that are no longer capable of functioning as FRET acceptors. Incomplete maturation of the red fluorescent protein mCherry adds to the complexity of the system, as the non-matured mCherry has spectral properties similar to EGFP. EYFP would then be a better donor molecule than EGFP.

In order to fine tune FRET experiments, it is very important to use a VFP donor where the same linking peptide is present as in the construct. Usually the free VFP without linking peptide is used as donor molecule. However, when the connecting peptide is introduced, the chromophore in the VFP may sense a different molecular environment that is reflected in a slightly different lifetime. A good example is ECFP, whose long lifetime distribution is rather broad and sensitive to slight external variations (compare ECFP results in Tables 1, 2). Measurements of a total construct without acceptor would remove any ambiguity in the accurate determination of the fluorescence lifetime of the donor alone that is always required for quantitative FRET measurements.

These studies have demonstrated that FRET–FLIM studies in living cells lead to overestimated distances, i.e. they are too long. If one were only interested in a yes-or-no answer, then this would be a first approximation. However, when physical techniques are applied to biological problems, we must always strive for a quantitative description of the results and, consequently, an improved analysis of the experimental observations.

References

Albertazzi L, Arosio D, Marchetti L, Ricci F, Beltram F (2009) Quantitative FRET analysis with the EGFP-mCherry fluorescent protein pair. Photochem Photobiol 85:287–297

Alberts B (1998) The cell as a collection of protein machines: preparing the next generation of molecular biologists. Cell 92:291–294

Bae JH, Rubini M, Jung G, Wiegand G, Seifert MH, Azim MK, Kim JS, Zumbusch A, Holak TA, Moroder L, Huber R, Budisa N (2003) Expansion of the genetic code enables design of a novel "gold" class of green fluorescent proteins. J Mol Biol 328:1071–1081

Barber PR, Ameer-Beg S, Gilbey J, Carlin LM, Keppler M, Ng TC, Vojnovic B (2009) Multiphoton time-domain fluorescence lifetime imaging microscopy: practical application to protein–protein interactions using global analysis. J R Soc Interface 6:S93–S105

Bastiaens PIH, van Hoek A, Wolkers WF, Brochon JC, Visser AJWG (1992a) Comparison of the dynamic structures of lipoamide dehydrogenase and glutathione reductase by time-resolved polarized flavin fluorescence. Biochemistry 31:7050–7060

Bastiaens PIH, van Hoek A, Benen JAE, Brochon JC, Visser AJWG (1992b) Conformational dynamics and intersubunit energy transfer in wild-type and mutant lipoamide dehydrogenase from *Azotobacter vinelandii*. A multidimensional time-resolved polarized fluorescence study. Biophys J 63:839–853

Borst JW, Hink MA, van Hoek A, Visser AJWG (2005) Effects of refractive index and viscosity on fluorescence and anisotropy decays of enhanced cyan and yellow fluorescent proteins. J Fluoresc 15:153–160

Borst JW, Laptenok SP, Westphal AH, Kühnemuth R, Hornen H, Visser NV, Kalinin S, Aker J, van Hoek A, Seidel CAM, Visser AJWG (2008) Structural changes of yellow cameleon domains observed by quantitative FRET analysis and polarized fluorescence correlation spectroscopy. Biophys J 95:5399–5411

Brochon JC (1994) Maximum entropy method of data analysis in time-resolved spectroscopy. Methods Enzymol 240:262–311

Cotlet M, Hofkens J, Habuchi S, Dirix G, Van Guyse M, Michiels J, Vanderleyden J, De Schryver FC (2001) Identification of different emitting species in the red fluorescent protein DsRed by means of ensemble and single-molecule spectroscopy. Proc Natl Acad Sci USA 98:14398–14403

Day RN, Booker CF, Periasamy A (2008) Characterization of an improved donor fluorescent protein for Forster resonance energy transfer microscopy. J Biomed Opt 13:031203

Elder AD, Domin A, Schierle GSK, Lindon C, Pines J, Esposito A, Kaminski CF (2009) A quantitative protocol for dynamic measurements of protein interactions by Förster resonance energy transfer-sensitised fluorescence emission. J R Soc Interface 6:S59–S81

Esposito A, Gralle M, Dani MA, Lange D, Wouters FS (2008) pHlameleons: a family of FRET-based protein sensors for quantitative pH imaging. Biochemistry 47:13115–13126

Evers TH, van Dongen EMWM, Faesen AC, Meijer EW, Merkx M (2006) Quantitative understanding of the energy transfer between fluorescent proteins connected via flexible linkers. Biochemistry 45:13183–13192

Festy F, Ameer-Beg SM, Ng T, Suhling K (2007) Imaging proteins in vivo using fluorescence lifetime microscopy. J R Soc Mol Biosyst 3:381–391

Förster T (1948) Zwischenmolekulare Energiewanderung und Fluoreszenz. Ann Phys 2:55–75

Giepmans BN, Adams SR, Ellisman MH, Tsien RY (2006) The fluorescent toolbox for assessing protein location and function. Science 312:217–224

Grinvald A, Haas E, Steinberg IZ (1972) Evaluation of distribution of distances between energy donors and acceptors by fluorescence decay. Proc Natl Acad Sci USA 69:2273–2277

Haas E, Wilchek M, Katchalski-Katzir E, Steinberg IZ (1975) Distribution of end-to-end distances of oligopeptides in solution as estimated by energy-transfer. Proc Natl Acad Sci USA 72:1807–1811

Heikal AA, Hess ST, Webb WW (2001) Multiphoton molecular spectroscopy and excited-state dynamics of enhanced green

fluorescent protein (EGFP): acid–base specificity. Chem Phys 274:37–55

Hess ST, Sheets ED, Wagenknecht-Wiesner A, Heikal AA (2003) Quantitative analysis of the fluorescence properties of intrinsically fluorescent proteins in living cells. Biophys J 85:2566–2580

Jares-Erijman EA, Jovin TM (2003) FRET imaging. Nat Biotechnol 21:1387–1395

Jares-Erijman EA, Jovin TM (2006) Imaging molecular interactions in living cells by FRET microscopy. Curr Opin Chem Biol 10:409–416

Jose M, Nair DK, Reissner C, Hartig R, Zuschratter W (2007) Photophysics of clomeleon by FLIM: discriminating excited state reactions along neuronal development. Biophys J 92:2237–2254

Kaminski C (2009) Quantitative fluorescence microscopy. J R Soc Interface 6:S1–S2

Kirber MT, Chen K, Keaney JF (2007) YFP photoconversion revisited: confirmation of the CFP-like species. Nat Methods 4:767–768

Kremers GJ, Hazelwood KL, Murphy CS, Davidson MW, Piston DW (2009) Photoconversion in orange and red fluorescent proteins. Nat Methods 6:355–358

Livesey AK, Brochon JC (1987) Analyzing the distribution of decay constants in pulse-fluorometry using the maximum-entropy method. Biophys J 52:693–706

Maeder CI, Hink MA, Kinkhabwala A, Mayr R, Bastiaens PIH, Knop M (2007) Spatial regulation of Fus3 MAP kinase activity through a reaction–diffusion mechanism in yeast pheromone signalling. Nat Cell Biol 9:1319–1326

Merola F, Rigler R, Holmgren A, Brochon JC (1989) Picosecond tryptophan fluorescence of thioredoxin: evidence for discrete species in slow exchange. Biochemistry 28:3383–3398

Millington M, Grindlay GJ, Altenbach K, Neely RK, Kolch W, Bencina M, Read ND, Jones AC, Dryden DT, Magennis SW (2007) High-precision FLIM-FRET in fixed and living cells reveals heterogeneity in a simple CFP-YFP fusion protein. Biophys Chem 127:155–164

Miyawaki A, Llopis J, Heim R, McCaffery JM, Adams JA, Ikura M, Tsien RY (1997) Fluorescent indicators for Ca^{2+} based on green fluorescent proteins and calmodulin. Nature 388:882–887

Miyawaki A, Griesbeck O, Heim R, Tsien RY (1999) Dynamic and quantitative Ca^{2+} measurements using improved cameleons. Proc Natl Acad Sci USA 96:2135–2140

Miyawaki A, Sawano A, Kogure T (2003) Lighting up cells: labelling proteins with fluorophores. Nat Cell Biol 5(Suppl):S1–S7

Nagai T, Yamada S, Tominaga T, Ichikawa M, Miyawaki A (2004) Expanded dynamic range of fluorescent indicators for Ca^{2+} by circularly permuted yellow fluorescent proteins. Proc Natl Acad Sci USA 101:10554–10559

Patterson GH, Lippincott-Schwartz J (2002) A photoactivatable GFP for selective photolabeling of proteins and cells. Science 297:1873–1877

Peter M, Ameer-Beg SM, Hughes MK, Keppler MD, Prag S, Marsh M, Vojnovic B, Ng T (2005) Multiphoton-FLIM quantification of the EGFP-mRFP1 FRET pair for localization of membrane receptor-kinase interactions. Biophys J 88:1224–1237

Shaner NC, Campbell RE, Steinbach PA, Giepmans BN, Palmer AE, Tsien RY (2004) Improved monomeric red, orange and yellow fluorescent proteins derived from *Discosoma* sp. red fluorescent protein. Nat Biotechnol 22:1567–1572

Shaner NC, Steinbach PA, Tsien RY (2005) A guide to choosing fluorescent proteins. Nat Methods 2:905–909

Suhling K, Siegel J, Phillips D, French PMW, Leveque-Fort S, Webb SE, Davis DM (2002) Imaging the environment of green fluorescent protein. Biophys J 83:3589–3595

Tramier M, Zahid M, Mevel JC, Masse MJ, Coppey-Moisan M (2006) Sensitivity of CFP/YFP and GFP/mCherry pairs to donor

photobleaching on FRET determination by fluorescence lifetime imaging microscopy in living cells. Microsc Res Tech 69:933–939

Tsien RY (1998) The green fluorescent protein. Annu Rev Biochem 67:67509–67544

Uskova MA, Borst JW, Hink MA, van Hoek A, Schots A, Klyachko NL, Visser AJWG (2000) Fluorescence dynamics of green fluorescent protein in AOT reversed micelles. Biophys Chem 87:73–84

Valentin G, Verheggen C, Piolot T, Neel H, Coppey-Moisan M, Bertrand E (2005) Photoconversion of YFP into a CFP-like species during acceptor photobleaching FRET experiments. Nat Methods 2:801

van den Berg PAW, van Hoek A, Walentas CD, Perham RN, Visser AJWG (1998) Flavin fluorescence dynamics and photoinduced electron transfer in *Escherichia coli* glutathione reductase. Biophys J 74:2046–2058

van den Berg PAW, Mulrooney SB, Gobets B, van Stokkum IHM, van Hoek A, Williams CH, Visser AJWG (2001) Exploring the conformational equilibrium of *E. coli* thioredoxin reductase: characterization of two catalytically important states by ultrafast flavin fluorescence spectroscopy. Protein Sci 10:2037–2049

van Hoek A, Vos K, Visser AJWG (1987) Ultrasensitive time-resolved polarized fluorescence spectroscopy as a tool in biology and medicine. J Quant Electr 23:1812–1820

Varadi A, Rutter GA (2002) Green fluorescent protein calcium biosensors. Calcium imaging with GFP cameleons. Methods Mol Biol 183:255–264

Verkhusha VV, Lukyanov KA (2004) The molecular properties and applications of Anthozoa fluorescent proteins and chromoproteins. Nat Biotechnol 22:289–296

Villoing A, Ridhoir M, Cinquin B, Erard M, Alvarez L, Vallverdu G, Pernot P, Grailhe R, Merola F, Pasquier H (2008) Complex fluorescence of the cyan fluorescent protein: comparisons with the H148D variant and consequences for quantitative cell imaging. Biochemistry 47:12483–12492

Vogel SS, Thaler C, Koushik SV (2006) Fanciful FRET. Sci STKE 2006:re2

Wlodarczyk J, Woehler A, Kobe F, Ponimaskin E, Zeug A, Neher E (2008) Analysis of FRET signals in the presence of free donors and acceptors. Biophys J 94:986–1000

Wu PG, Brand L (1992) Orientation factor in steady-state and time-resolved resonance energy-transfer measurements. Biochemistry 31:7939–7947

Wu PG, Rice KG, Brand L, Lee YC (1991) Differential flexibilities in 3 branches of an N-linked triantennary glycopeptide. Proc Natl Acad Sci USA 88:9355–9359

Zhang J, Campbell RE, Ting AY, Tsien RY (2002) Creating new fluorescent probes for cell biology. Nat Rev Mol Cell Biol 3:906–918